Critical collapse in Einstein-Gauss-Bonnet gravity in five and six dimensions

N. Deppe,[1] C. D. Leonard,[3,4] T. Taves,[2,6] G. Kunstatter,[1,2] and R. B. Mann[3,5]

[1]*Department of Physics and Astronomy, University of Winnipeg, Winnipeg, Manitoba R3B 2E9, Canada*
[2]*Winnipeg Institute of Theoretical Physics, Winnipeg, Manitoba R3B 2E9, Canada*
[3]*Department of Physics and Astronomy, University of Waterloo, Waterloo, Ontario N2L 3G1, Canada*
[4]*Department of Physics and Physical Oceanography, Memorial University of Newfoundland, Saint John's, Newfoundland A1B 3X7, Canada*
[5]*Perimeter Institute, 31 Caroline Street North, Waterloo, Ontario N2L 2Y5, Canada*
[6]*Department of Physics and Astronomy, University of Manitoba, Winnipeg, Manitoba R3T 2N2, Canada*

(Received 6 September 2012; published 5 November 2012)

Einstein-Gauss-Bonnet gravity provides a natural higher dimensional and higher order curvature generalization of Einstein gravity. It contains a new, presumably microscopic, length scale that should affect short distance properties of the dynamics, such as Choptuik scaling. We present the results of a numerical analysis in generalized flat slice coordinates of self-gravitating massless scalar spherical collapse in five and six dimensional Einstein-Gauss-Bonnet gravity near the threshold of black hole formation. Remarkably, the behavior is universal (i.e., independent of initial data) but qualitatively different in five and six dimensions. In five dimensions there is a minimum horizon radius, suggestive of a first order transition between black hole and dispersive initial data. In six dimensions no radius gap is evident. Instead, below the Gauss-Bonnet scale there is a change in the critical exponent and echoing period.

DOI: 10.1103/PhysRevD.86.104011 PACS numbers: 04.70.Bw, 04.50.−h

I. INTRODUCTION

Recent interest in string theory has popularized the study of higher dimensional and higher curvature gravity. The Einstein action has many desirable properties: it is second order in derivatives of the metric, ghost free when linearized about a flat background and obeys a Birkhoff theorem that yields a one parameter family of spherically symmetric black hole solutions. In four dimensions the Ricci scalar is the only curvature invariant with these properties but in dimensions greater than four it is possible to add higher order curvature terms in the form of so-called Lovelock polynomials [1–3]. These terms contribute to the equations of motion while retaining no more than second derivatives of the metric. Moreover, they have been proven to be ghost free [4] and obey a generalized Birkhoff theorem [5,6].

The Lovelock action, I, written in terms of the Lovelock polynomials, $\mathcal{L}_{(p)}$, is given by

$$I = \frac{1}{2\kappa_n^2}\int d^n x\sqrt{-g}\sum_{p=0}^{[n/2]}\alpha_{(p)}\mathcal{L}_{(p)}, \tag{1.1}$$

$$\mathcal{L}_{(p)} = \frac{p!}{2^p}\delta^{\mu_1\ldots\mu_p\nu_1\ldots\nu_p}_{\rho_1\ldots\rho_p\sigma_1\ldots\sigma_p}\mathcal{R}_{\mu_1\nu_1}{}^{\rho_1\sigma_1}\ldots\mathcal{R}_{\mu_p\nu_p}{}^{\rho_p\sigma_p}, \tag{1.2}$$

where $\kappa_n = \sqrt{8\pi G_n}$, G_n is Newton's gravitational constant, g is the determinant of the metric, n is the number of spacetime dimensions, $[n/2]$ refers to the largest integer less than $n/2$, $\delta^{\mu_1\ldots\mu_p}_{\rho_1\ldots\rho_p} := \delta^{\mu_1}_{[\rho_1}\ldots\delta^{\mu_p}_{\rho_p]}$ and $\mathcal{R}_{\mu\nu\rho\sigma}$ is the Riemann curvature tensor. $\alpha_{(p)}$ are coupling constants of dimension (length)$^{2(p-1)}$. The first two terms, $\mathcal{L}_{(0)}$ and $\mathcal{L}_{(1)}$, correspond to the cosmological constant and Einstein-Hilbert term, respectively, while $\mathcal{L}_{(2)}$ is the Gauss-Bonnet (GB) term. It has been argued [7] that the GB term appears in the low-energy limit for strings propagating in curved spacetime. Here we focus on the simplest nontrivial theory, namely Einstein-Gauss-Bonnet (EGB) gravity, containing only the Einstein term and $p = 2$ GB term.[1]

It has been known for quite some time that the spherically symmetric collapse of a massless scalar field minimally coupled to general relativity (GR) exhibits critical behavior [8]. Specifically, numerical studies of black hole formation indicate that for any parameter in the initial data, A say, there exists a corresponding critical value A^* such that for $A > A^*$ a black hole forms while for $A < A^*$ the matter disperses to infinity. Black holes with A just slightly bigger than A^* are known as near critical black holes. Near criticality all geometrical quantities describing the black hole, such as its mass, obey a scaling relation of the form

$$\ln(M_{\mathrm{BH}}) = \gamma\ln(A - A^*) + f(A - A^*), \tag{1.3}$$

where f is a periodic function of its argument. The critical exponent γ and the period T of f are universal[2] in the

[1]The addition of a cosmological constant should not affect the short distance behavior that is the subject of our paper.

[2]γ depends only on the scaling dimension of the quantity considered. For example in 4D M scales as length so the radius and mass of the black hole have the same critical exponent. Curvature, on the other hand, scales as (length)^2, so its critical exponent is double that of mass.

sense that they are independent of the form of the initial data or the specifics of the parameter A that is varied. This universality and the vanishing of $M_{\rm BH}$ at criticality [cf. Eq. (1.3)] suggest a second order phase transition between the black hole and dispersive end states of the collapse. This fascinating behavior was ultimately explained using renormalization group arguments in the context of radiation fluids [9]. For spherical massless scalar field collapse, the critical exponent and echoing period were obtained by Gundlach [10] from the properties of a critical, discretely self-similar zero mass black hole solution that behaves like an intermediate attractor in the space of solutions.

The critical exponent γ and period T do depend on the number of dimensions and the type of matter. In addition, the form of f can depend on the spacetime slicing and the particular quantity that is being measured. For example, in Schwarzschild and null coordinates the radius of the horizon on formation yields an f that is well fit to a small amplitude sine wave. By comparison, in flat slice or Painlevé-Gullstrand (PG) coordinates the periodic function that describes the scaling of the apparent horizon on formation exhibits large amplitude cusps [11,12]. The difference can be understood by noting that in the former case one is measuring a quantity very close to the radius of the final event horizon, whereas in PG coordinates the apparent horizon is detected much earlier. The large amplitude cusps are likely due to that fact that near criticality in PG coordinates the apparent horizon forms at small radius and hence in the strong field region where such large fluctuations are expected.[3] On the other hand the scaling relation for the maximum value of the Ricci scalar at the origin for subcritical evolution is invariant and exhibits slicing independent small oscillations.

The presence of a dimensionful constant in the action in general changes the above scenario, as verified for Yang-Mills collapse [13], massive scalar field collapse [14] and massive gauge field collapse [15]. In massive scalar field collapse, for initial data whose width is smaller than the Compton wavelength of the scalar field, the usual second order phase transition is found, whereas in the other limit the phase transition exhibits a mass gap and is first order. It is clearly of interest to study the effects on Choptuik scaling of the Gauss-Bonnet parameter and higher order Lovelock coupling constants. Golod and Piran [16] recently presented such an analysis for the spherical collapse of massless scalar matter coupled to EGB gravity in five dimensions using double null coordinates. They found, as expected, that the Gauss-Bonnet term dominates the dynamics at short distances and destroys the discrete self-similarity characteristic of Choptuik scaling. Their work concentrated on the regime where the GB terms strongly dominated the dynamics.

[3]We are grateful to Patrick Brady for suggesting this explanation.

The purpose of the present work is to investigate further the critical collapse of a spherically symmetric, massless scalar field minimally coupled to five and six dimensional EGB gravity. We work in flat slice or generalized PG coordinates since they have several advantages over double null coordinates in the present context: They are regular at apparent horizons so that the simulations can run up to (and even past) horizon formation. Hence one can calculate the time and position of horizon formation without having to stop the code at some arbitrary distance before horizon formation as would be necessary in Schwarzschild and null coordinates. More importantly, the cusplike nature of the horizon scaling function in PG coordinates has the advantage of making the potential appearance of the periodicity in an equation such as (1.3) more obvious. It should be pointed out that one disadvantage of using PG coordinates is the lack of automatic spatial mesh refinement which occurs near horizon formation in null coordinates. As we will explain in the next section, the nature of the dynamical equations suggest that qualitative differences can occur in different numbers of spacetime dimensions. It is for this reason that we investigate both five and six spacetime dimensions.

We confirm some of the results in five dimensions [16], extend the analysis to six dimensions and obtain some surprising new results in both five and six dimensions. For all initial data and choice of parameter A that we examined there exists a critical value A^* that separates black hole formation from dispersion. As expected, when the horizon forms far from the singularity the GR term dominates and the standard Choptuik critical scaling relation is found. Things change as one gets close enough to criticality to enter the region in which the GB terms dominate the dynamics. Near criticality the scalar field at the origin oscillates with a constant period T that converges as $(A - A^*) \to 0$ to a value that depends on the GB parameter as previously shown [16]. We find a different relationship between T and the GB parameter than in Ref. [16], albeit for smaller values of the GB parameter.

In addition, we explore in detail the scaling in the GB dominated region. We find qualitatively different behavior in five and six dimensions. In five dimensions there is evidence for a radius gap: in the supercritical region the radius of the apparent horizon on formation asymptotes to a constant value as criticality is approached from above. The maximum value of the Ricci scalar at the origin also appears to approach a constant value as criticality is approached from below.

In six dimensions, the behavior is qualitatively different. In the GB region the radius of the apparent horizon formation obeys a relationship similar to (1.3) but with different exponent and period. The maximum Ricci scalar also exhibits this same scaling relation with another scaling exponent, and small, but irregular oscillations.

The rest of this work is organized as follows. In Sec. II, we describe the equations of motion which we derived

using Hamiltonian formalism [17]. In Sec. III, we discuss the numerical implementation of the solution and describe the general methods used to obtain results. In Sec. IV, we give our results and we conclude in Sec. V.

II. EQUATIONS OF MOTION

As stated above, we start with the action for a massless scalar field ψ minimally coupled to the EGB action:

$$I = \frac{1}{2\kappa_n^2}\int d^n x\sqrt{-g}(\mathcal{R} + \alpha_{(2)}[\mathcal{R}^2 - 4\mathcal{R}_{\mu\nu}\mathcal{R}^{\mu\nu} + \mathcal{R}_{\mu\nu\rho\sigma}\mathcal{R}^{\mu\nu\rho\sigma}] + \kappa_n^2(\nabla\psi)^2). \tag{2.1}$$

We use the Arnowitt-Deser-Misner metric parametrization:

$$ds^2 = -N^2(x,t)dt^2 + \Lambda^2(x,t)(dx + N_r(x,t)dt)^2 + R^2(x,t)d\Omega^2, \tag{2.2}$$

where R is the areal radius. It is also useful to define the Misner-Sharp mass function [18], suitably generalized to EGB [19]:

$$\mathcal{M} := \frac{1}{2kG}[R^{n-3}(1 - (DR)^2) + \tilde{\alpha}_{(2)}R^{n-5}(1 - (DR)^2)^2], \tag{2.3}$$

where the n dimensional gravitational constant, G, is defined as $2kG = 2\kappa_n^2/(n-2)A_{n-2}$ [11], A_{n-2} is the surface area of an $n-2$ dimensional sphere, $k = 8(n-3)/(n-2)^2$, D is the two dimensional covariant derivative and $\tilde{\alpha}_{(2)} := ((n-3)!/(n-5)!)\alpha_{(2)}$. In the following we work in units in which $2G = 1$. We work in flat slice coordinates $x = R$ and $\Lambda = 1$ in which the equations of motion for the scalar field and its conjugate momentum are [17]

$$\dot{\psi} = N\left(\frac{\Pi_\psi}{R^{n-2}} + \left(\frac{N_r}{N}\right)\psi'\right) \tag{2.4}$$

and

$$\dot{\Pi}_\psi = \left[N(R^{n-2}\psi' + \left(\frac{N_r}{N}\right)\Pi_\psi\right)\Big]', \tag{2.5}$$

where dots and primes represent differentiation with respect to t and R respectively. Preservation of the gauge condition $R = x$ in time determines the shift algebraically in terms of the lapse, the areal radius and the mass function:

$$\mathcal{M} := \frac{1}{2kG}\left[R^{n-3}\left(\frac{N_r}{N}\right)^2 + \tilde{\alpha}_{(2)}R^{n-5}\left(\frac{N_r}{N}\right)^4\right]. \tag{2.6}$$

This can be solved algebraically and yields, for EGB gravity,

$$\frac{N_r}{N} = \sqrt{\frac{R^2}{\tilde{\alpha}}\left(\sqrt{1 + \frac{2\tilde{\alpha}}{R^2}\frac{2kG\mathcal{M}}{R^{n-3}}} - 1\right)}, \tag{2.7}$$

where we have defined $\tilde{\alpha} := 2(n-4)(n-3)\alpha_{(2)}$ for purposes which will become obvious later. The sign of the inner square root in the above has been chosen to give the correct GR limit as $\tilde{\alpha} \to 0$.

The consistency condition $\dot{\Lambda} = 0$ determines the lapse via

$$N' = -\frac{kGN\Pi_\psi\psi'}{R^{n-3}}\Big/\left(\left(\frac{N_r}{N}\right)\left(1 + \frac{\tilde{\alpha}}{R^2}\left(\frac{N_r}{N}\right)^2\right)\right), \tag{2.8}$$

while the Hamiltonian constraint then takes the form

$$\mathcal{M}' = \frac{1}{2}\left(\frac{\Pi_\psi^2}{R^{n-2}} + R^{n-2}\psi'^2\right) + \left(\frac{N_r}{N}\right)\Pi_\psi\psi'. \tag{2.9}$$

Using (2.7) to replace N_r/N by $\mathcal{M}$ in (2.9) provides a differential equation that can be solved for $\mathcal{M}$ and hence N_r/N in terms of the scalar field and its conjugate momenta on each spatial slice.

Given the solution for $\mathcal{M}$, one can look for apparent horizons by solving (2.3) for $(DR)^2 = 0$. In our coordinates, this becomes simply

$$AH := 1 - \left(\frac{N_r}{N}\right)^2 = 0, \tag{2.10}$$

where for ease of reference we refer to AH as the horizon function. For EGB, one can also use (2.6) and the above to obtain

$$\mathcal{M}(R_{AH}) = \frac{1}{4kG}(\tilde{\alpha}R_{AH}^{n-5} + 2R_{AH}^{n-3}). \tag{2.11}$$

Note that in 5D the first term is constant so that there is an algebraic lower bound on the black hole mass as the radius of the horizon goes to zero.

Our goal is to solve the time evolution equations (2.4) and (2.5) for the scalar field and its conjugate momentum, with N and N_r/N on each time slice determined using (2.7), (2.8), and (2.9) and then use (2.11) to look for the formation of an apparent horizon.

The actual time evolution equation as implemented in the code was obtained by expanding the derivative in (2.5) and replacing the derivatives of $\mathcal{M}'$ and N' using Eqs. (2.7) and (2.9). This gives

$$\dot{\Pi}_\psi = N\Big\{\Big[Gk\left(\frac{\Pi_\psi^3}{2R^{2n-5}} - \frac{\psi'^2\Pi_\psi R}{2}\right)\Big/\left(\frac{N_r}{N}\right) + -\frac{(n-3)\Pi_\psi}{2R}\left(\frac{N_r}{N}\right) - \frac{\tilde{\alpha}(n-5)\Pi_\psi}{4R^3}\left(\frac{N_r}{N}\right)^3\Big]\Big/\left(1 + \frac{\tilde{\alpha}}{R^2}\left(\frac{N_r}{N}\right)^2\right) + (n-2)R^{n-3}\psi' + R^{n-2}\psi'' + \Pi_\psi'\left(\frac{N_r}{N}\right)\Big\}. \tag{2.12}$$

Note that in five spacetime dimensions the last term proportional to $1/R^3$ in the square brackets above vanishes. One might therefore expect behavior for $n > 5$ that is qualitatively different from $n = 5$. It is for this reason that it is important to study higher dimensions. In the present paper we restrict consideration to five and six dimensions.

III. NUMERICS AND METHODS

The system is evolved using C + + code as follows:

(1) Initialize the spatial lattice. We set the lattice spacing to 10^{-5} (unless otherwise stated) for the first 100 points near the origin and then slowly increase it to 10^{-2} at the 1200th and final lattice point.

(2) Set up initial conditions. We initialized Π_ψ to zero and ψ to be either a Gaussian ψ_G or hyperbolic tangent ψ_H as follows:

$$\psi_G = AR^2 \exp\left[-\left(\frac{R-R_0}{B}\right)^2\right];$$
$$\psi_H = A\tanh\left[\frac{R-R_0}{B}\right], \tag{3.1}$$

where A, B and R_0 are parameters.

(3) At $R=0$ set $N=1$, $\mathcal{M}=0$ and use a subroutine to calculate N_r/N using Eq. (2.7). Integrate N and $\mathcal{M}$ forward in R using Eqs. (2.7), (2.8), and (2.9). This is done using a fourth order Runge-Kutta method. Spatial derivatives are calculated using a central difference routine except at the boundaries where forward and backward differences are used.

(4) Integrate ψ and Π_ψ forward in time using Eqs. (2.4), (2.5), and (2.7) employing a fourth order Runge-Kutta method. Stability is maintained by insisting that the size of the time step, $\Delta t(t)$, is determined by

$$\Delta t(t) < \min_R\left\{\left(\frac{dR}{dt}\right)^{-1}\Delta R(R)\right\}, \tag{3.2}$$

where $\Delta R(R)$ is the lattice spacing and $\frac{dR}{dt}$ is the maximum value of either the ingoing or outgoing local speed of light.

(5) Monitor the apparent horizon function, $AH := (DR)^2 = 1-(\frac{N_r}{N})^2$. At any point where $AH=0$, there is an apparent horizon. When AH forms a minimum it signals that an apparent horizon is soon to form, so the time steps are diminished by a factor of 10.

(6) Calculate the Ricci scalar and the mass density.

(7) Repeat steps 3–6 until the formation of an apparent horizon or until the field has dispersed.

For comparison purposes it was important that the code could simulate collapse without the GB term, i.e., in the GR case. It is not possible to take this limit when numerically calculating N_r/N using Eq. (2.7) so an if statement was added to the routine which calculates N_r/N in order to return $N_r/N = \sqrt{2kG\mathcal{M}/R^{n-3}}$ when $\tilde{\alpha}=0$.

When $\tilde{\alpha}$ is not zero a problem arises in the calculation of N_r/N when $4\tilde{\alpha}kG\mathcal{M}/R^{n-1}$ is sufficiently less than one. When this term is added to unity in the inner square root in (2.7), digits are lost and thus double precision cannot be claimed. For this reason a 16th order Taylor expansion of the inner square root in Eq. (2.7) was used in the case that $2\tilde{\alpha}2kG\mathcal{M}/R^{n-1} < 0.1$. Quadruple precision allowed for the investigation of overflow and underflow, as well as subtraction and addition round-off errors.

The code was capable of parallel processing, and many simulations were run on eight or more processors using the WestGrid and SHARCNET computing clusters. When generating data for mass and Ricci scaling plots the speed-up was linear with the number of processors used, whereas for the binary search used to find critical values the speed-up was logarithmic.

The critical value of a parameter in the initial conditions is defined as the value of that parameter for which a black hole just barely forms. We first performed a binary search to find the critical value of A in Eq. (3.1). $\psi(t, R=0)$ and $\mathcal{M}$ were then checked at late times to confirm that they blew up for A slightly bigger than A^* and remained finite for A slightly smaller than A^*. We were able to get consistent results to 12 significant figures. The A^* values for different values of $\tilde{\alpha}$ can be seen in Fig. 1. Interestingly the points are very well fit to

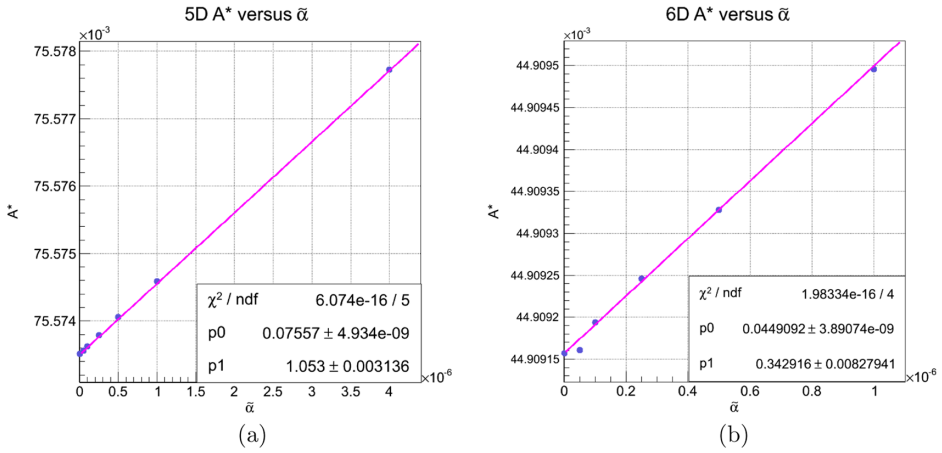

FIG. 1 (color online). A^* as a function of $\tilde{\alpha}$. (a) 5D. (b) 6D.

straight lines. The above procedure, of course, also gives B^* and R_0^*, which could also be varied. Using our values for A^* we calculated the wave function at the origin as a function of PG time and used these plots to find the period of oscillation near criticality, as a function of the $\tilde{\alpha}$.

We simulated matter bounce and dispersal for 280 simulations (the number 280 was chosen to optimize graph resolution and computing time) with $A < A^*$ and recorded the maximum value of the Ricci scalar $\mathcal{R}$ at $R = 0$ for each simulation. Plotting $\mathcal{R}_{\max}$ as a function of $A^* - A$ with a log-log scale gives the Ricci scaling plot. Similarly we simulated collapse for 280 simulations with $A > A^*$ and recorded the radius of the initial apparent horizon, R_{AH}. This procedure was repeated in five and six dimensions checking for scaling with both the A and B parameters in both the Gaussian and tanh initial data of Eq. (3.1) to check for universality. Using Gaussian initial data radius and Ricci scaling, plots were created for $\tilde{\alpha} = 10^{-8}$, 10^{-7}, 5×10^{-7}, 10^{-6} as well as the GR case $\tilde{\alpha} = 0$ to investigate the effects of the GB terms on the critical exponent, period and the existence of mass gap.

IV. RESULTS

A. Scalar field oscillations

In general relativity the discrete self-similarity of the critical solution results in oscillations of the scalar field at the origin with ever decreasing period. The presence of the dimensionful Gauss-Bonnet parameter breaks the scale invariance and the discrete self-similarity [16]. As shown in Figs. 2(b) and 3(b), the scalar field oscillations at the origin near criticality approach a constant period that depends on the value of the GB parameter. Since it was difficult to get close enough to criticality to guarantee that the period had converged, we plotted the values as a function of $\log(dA)$, where $dA \equiv |A - A^*|$. As seen in Figs. 2(c) and 3(c) the convergence was exponential and we used a best fit to determine the value of the period T and its corresponding error for each value of $\tilde{\alpha}$. The

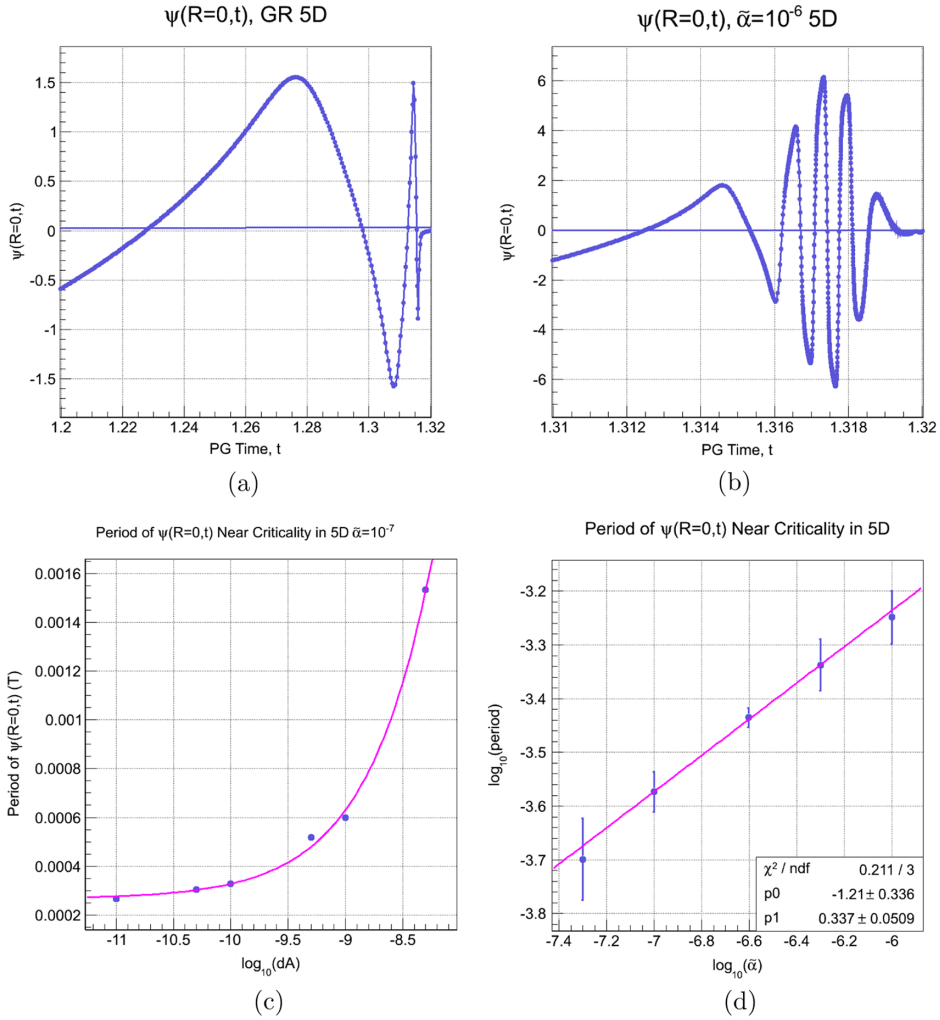

FIG. 2 (color online). Scalar field oscillations. (a) 5D, $\psi(0, t)$ near criticality, GR. (b) 5D, $\psi(0, t)$ near criticality, $\tilde{\alpha} = 10^{-6}$. (c) 5D, Period of $\psi(0, t)$ near criticality, $\tilde{\alpha} = 10^{-7}$, showing convergence. (d) Period of $\psi(0, t)$ in 5D near criticality as a function of GB parameter.

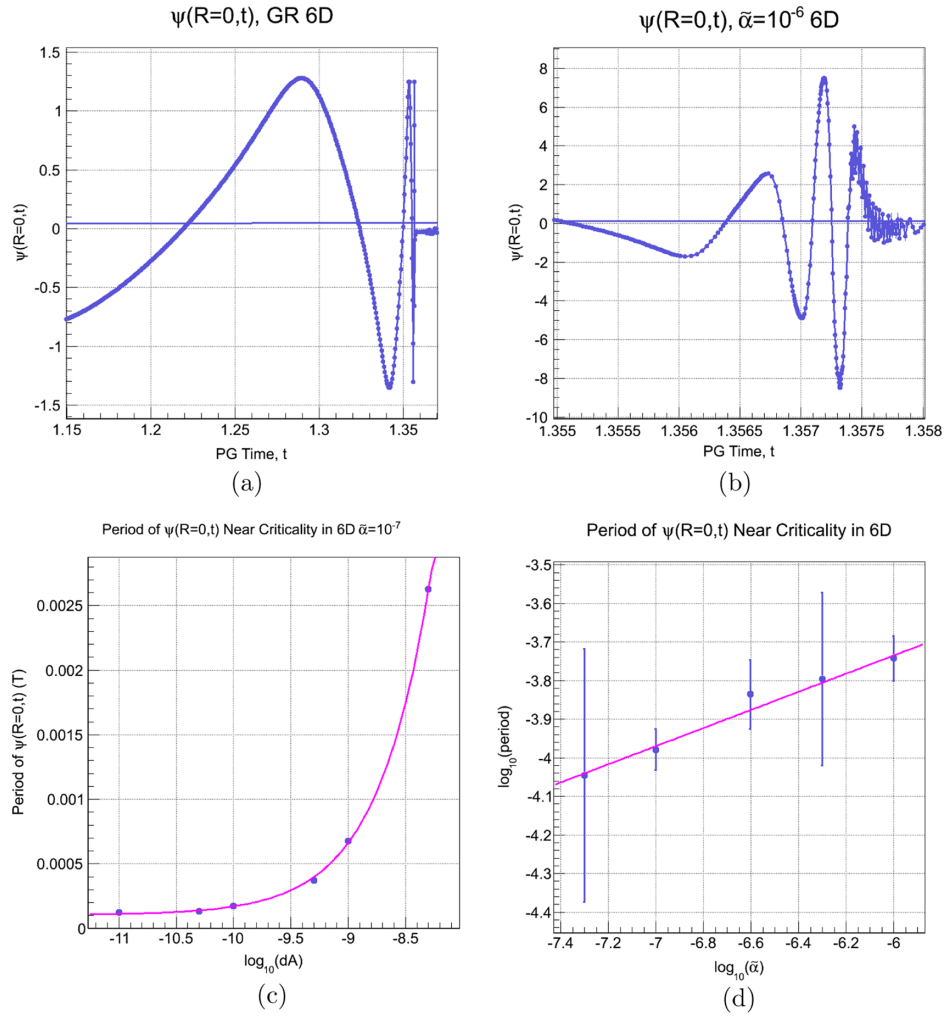

FIG. 3 (color online). Scalar field oscillations. (a) 6D, $\psi(0, t)$ near criticality, GR. (b) 6D, $\psi(0, t)$ near criticality, $\tilde{\alpha} = 10^{-6}$. (c) 6D, Period of $\psi(0, t)$ near criticality, $\tilde{\alpha} = 10^{-7}$, showing convergence. (d) Period of $\psi(0, t)$ in 6D near criticality as a function of GB parameter.

results are shown for five and six dimensions in Figs. 2(d) and 3(d). Our results are qualitatively similar to those in Ref. [16], namely

$$T_{(n)} \propto \tilde{\alpha}_{(n)}^{\beta}. \tag{4.1}$$

Our exponents in five and six dimensions are

$$\beta_{(5)} = 0.34 \pm 0.05, \tag{4.2}$$

$$\beta_{(6)} = 0.24 \pm 0.08. \tag{4.3}$$

These both differ from the value of approximately $1/2$ obtained in 5D by Golod and Piran [16], who argued that β is one divided by the scaling dimension of the GB coupling coefficient. Intriguingly our results suggest a relationship of

$$\beta_{(n)} = 1/(n-2). \tag{4.4}$$

Note that the 6D plots show oscillations at late times which are likely due to the buildup of numerical error.

We note also that the range of $\tilde{\alpha}$ that we considered was between 5×10^{-8} and 10^{-6}, which is outside the range 4×10^{-6} to 4×10^{-4} considered by Ref. [16], which may explain the discrepancy. We were restricted to smaller values of the GB parameter because our PG coordinate code did not allow us to get close enough to criticality for large values of $\tilde{\alpha}$ in order to reliably measure the period of the scalar field.

B. Critical exponents

In GR there exist universal scaling relations whose properties are determined in part by the critical solution. We now present two different sets of scaling plots in the GB case. The first is the value of the logarithm of the apparent horizon radius R_{AH} on formation as a function of $\log(dA)$ as the critical parameter is approached from above (i.e., supercritical). The second is the log of the maximum value of the Ricci scalar at the origin as a function of $\log(dA)$. We find as expected that if we are far enough

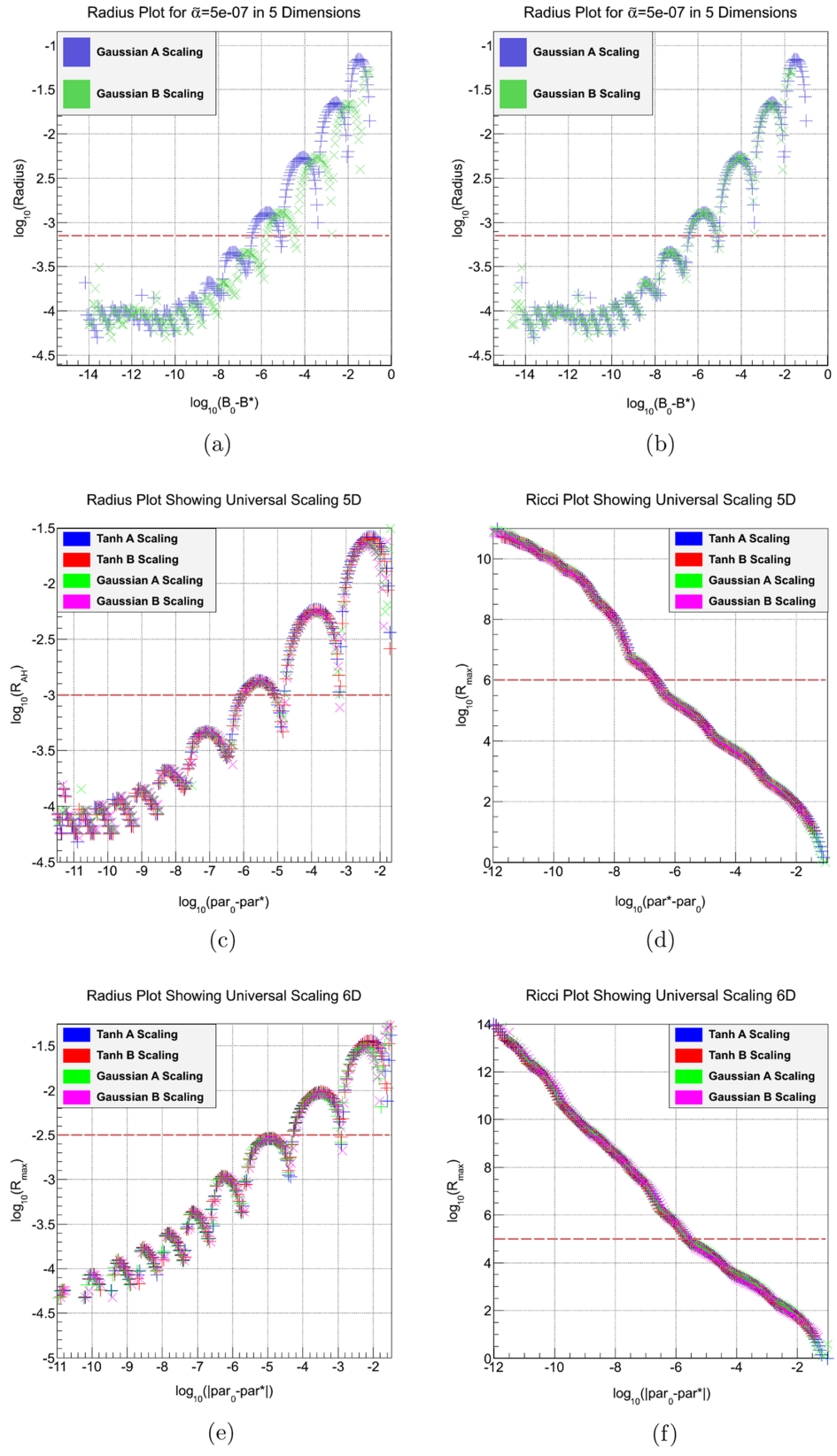

FIG. 4 (color online). Universality in 5D and 6D. (a) 5D, $\tilde{\alpha} = 5 \times 10^{-7}$, amplitude and width separately. (b) 5D, $\tilde{\alpha} = 5 \times 10^{-7}$, amplitude and width shifted to lie on top of each other. (c) 5D, $\tilde{\alpha} = 5 \times 10^{-7}$, Radius plots superimposed. (d) 5D, $\tilde{\alpha} = 5 \times 10^{-7}$, Ricci plots superimposed. (e) 6D, $\tilde{\alpha} = 10^{-5}$, Radius plots superimposed. (f) 6D, $\tilde{\alpha} = 10^{-5}$, Ricci plots superimposed.

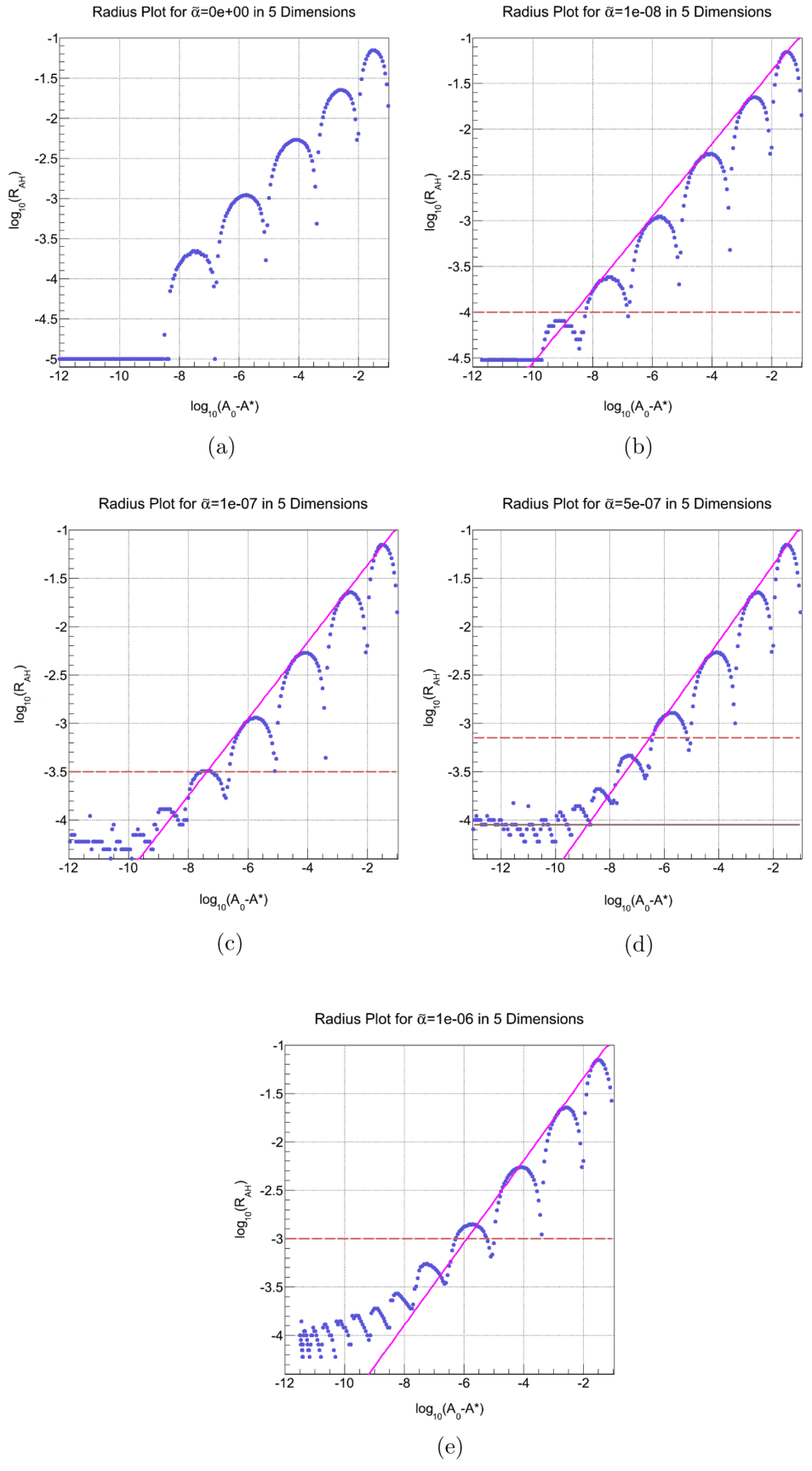

FIG. 5 (color online). Radius scaling plots (5D). The lines represent the best-fit tangents to the curves in their respective regimes. (a) GR, slope $= 0.413$. (b) $\tilde{\alpha} = 10^{-8}$. (c) $\tilde{\alpha} = 10^{-7}$. (d) $\tilde{\alpha} = 5 \times 10^{-7}$. (e) $\tilde{\alpha} = 10^{-6}$.

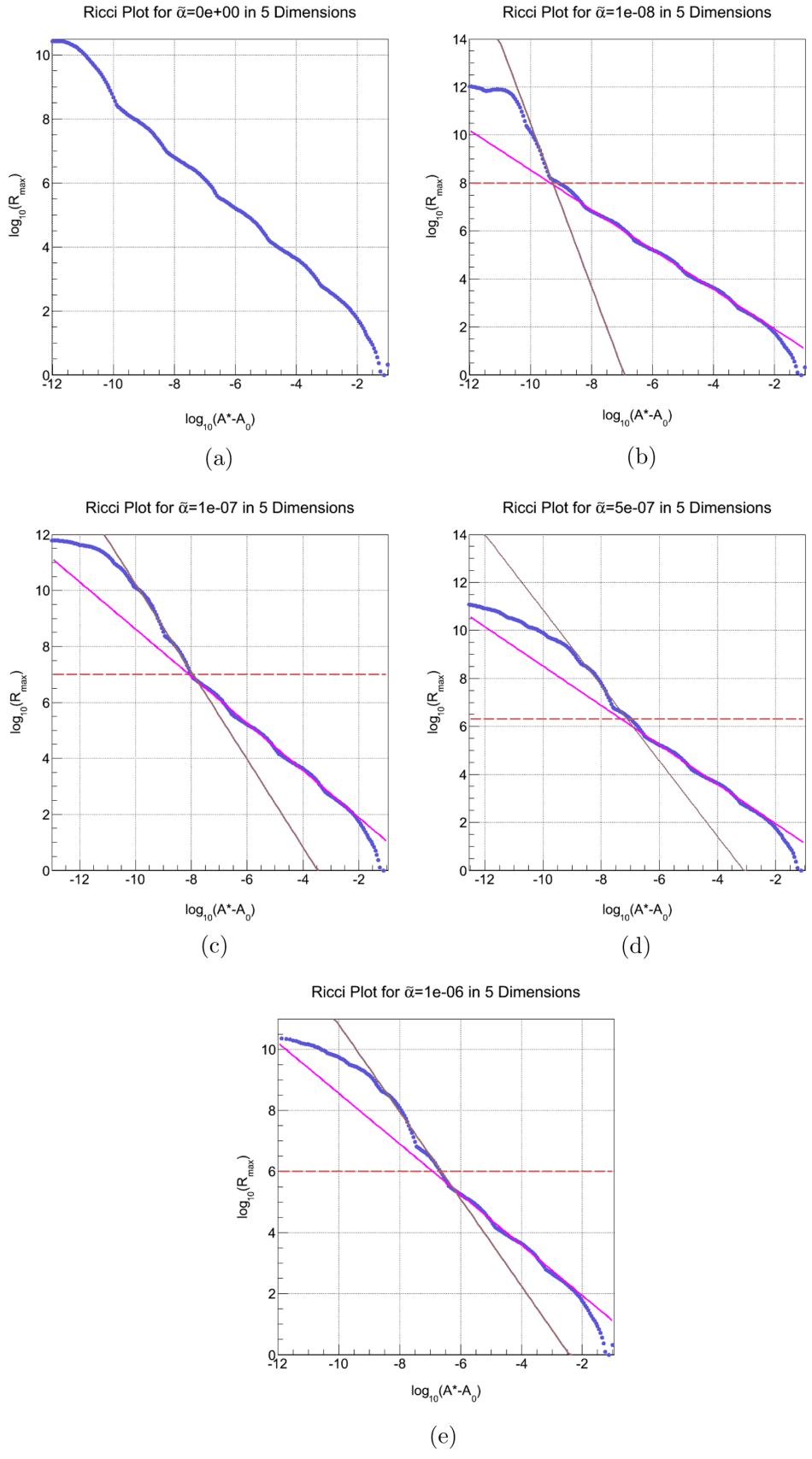

FIG. 6 (color online). Ricci scaling plots (5D). The lines represent the best-fit mean slopes of the curves in their respective regimes. (a) GR, slope $= 0.826$. (b) $\tilde{\alpha} = 10^{-8}$. (c) $\tilde{\alpha} = 10^{-7}$. (d) $\tilde{\alpha} = 5 \times 10^{-7}$. (e) $\tilde{\alpha} = 10^{-6}$.

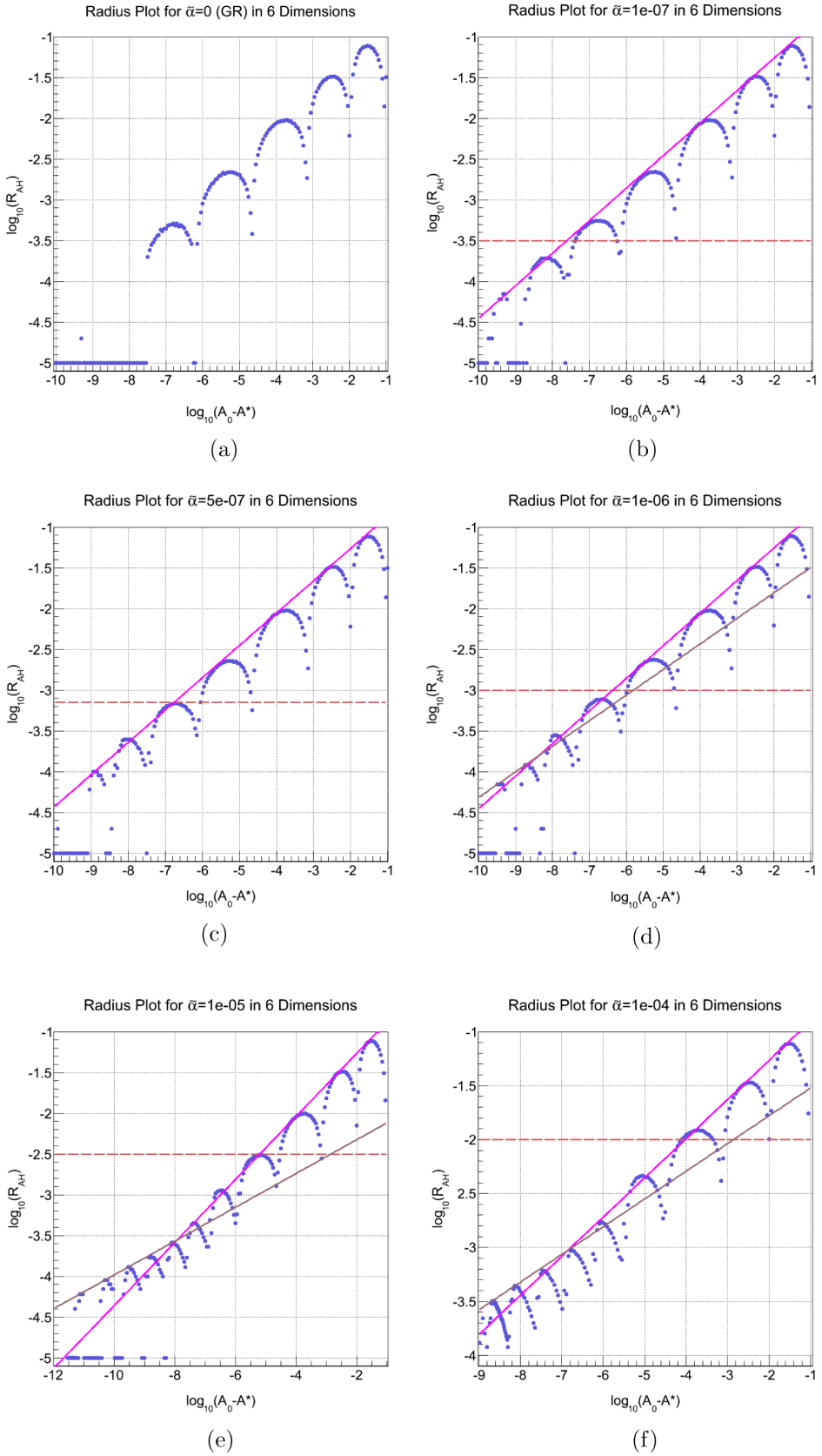

FIG. 7 (color online). Radius scaling plots (6D). The lines represent the best-fit tangents to the curves in their respective regimes. (a) GR, slope $= 0.43$. (b) $\tilde{\alpha} = 10^{-7}$. (c) $\tilde{\alpha} = 5 \times 10^{-7}$. (d) $\tilde{\alpha} = 10^{-6}$. (e) $\tilde{\alpha} = 10^{-5}$. (f) $\tilde{\alpha} = 10^{-4}$.

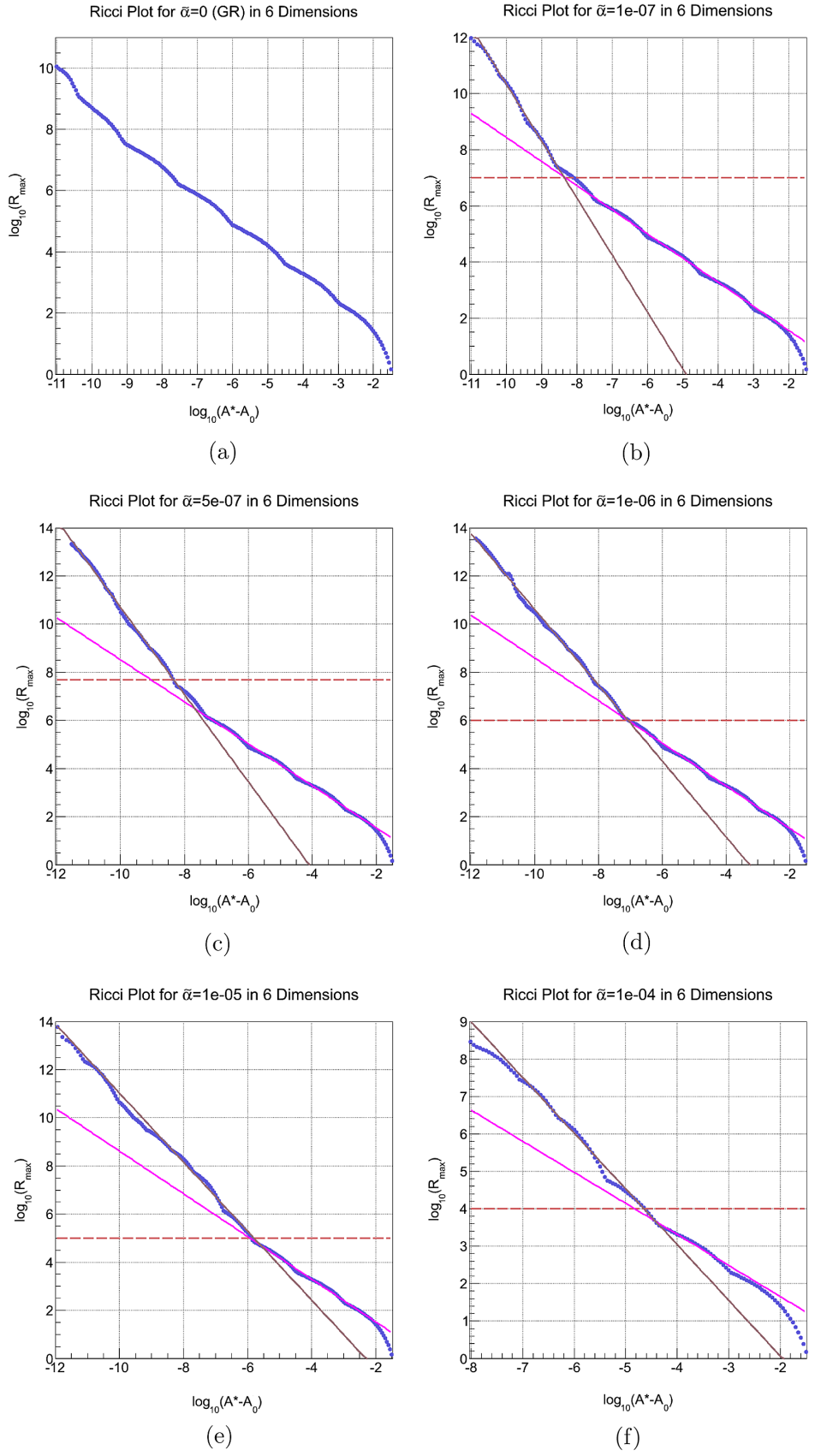

FIG. 8 (color online). Ricci scaling plots (6D). The lines represent the best-fit mean slopes of the curves in their respective regimes. (a) GR, slope $= 0.43$. (b) $\tilde{\alpha} = 10^{-7}$. (c) $\tilde{\alpha} = 5 \times 10^{-7}$. (d) $\tilde{\alpha} = 10^{-6}$. (e) $\tilde{\alpha} = 10^{-5}$. (f) $\tilde{\alpha} = 10^{-4}$.

from criticality that the curvatures stay small and the apparent horizon radius is large compared to the GB scale, we reproduce approximately the GR results: the curves are universal, with slope approximately equal to the GR critical exponent. The Ricci plots in this region are approximately straight lines with a small oscillation superimposed, whereas the radius plots show the large amplitude cusps observed in Refs. [12,20].

As the critical parameter is approached and we enter into the GB region things change, as can be seen in our scaling results illustrated in Figs. 4–8. In the case of the Ricci plots (Figs. 6 and 8), the GB region occurs when $\mathcal{R}\tilde{\alpha} > 1$, whereas for the radius plots (Figs. 5 and 7) it can be defined by the simpler relation $R_{AH} < \sqrt{\tilde{\alpha}}$. The boundary between the two regions is indicated in all the scaling plots by a horizontal dashed line.

The radius plots Figs. 5 and 7 continue to exhibit cusps, but with a decreased period and slope. The Ricci plots are also similar in the GB region to the GR region in that they are approximately straight lines with oscillations superimposed. However, the slope changes quite suddenly when the transition from GR to GB is made. The first important point is that the scaling plots are universal even in the GB region. This is illustrated for both 5D and 6D in Fig. 4. There are qualitative differences in the scaling plots between 5D and 6D so we will now discuss the two cases separately.

In the case of 5D there is evidence that the slope of the radius plot decreases continuously until a minimum radius is reached, i.e., that there is a radius gap. This is most evident in Fig. 6(d) but also appears to be the case in 6(e). In the remaining 5D figures the numerics did not allow us to probe deeply enough into the GB region to fully observe this.

A radius gap is not unexpected given the presence of the dimensionful GB parameter. Note that we focus on a radius gap instead of a mass gap because in 5D the former is trivial in light of (2.11).

The Ricci plots, initially approximately straight, change slope quite suddenly as one moves from the GR to the GB region, and then remain constant over a small range of $\log(dA)$. The slopes are given in Table I. As criticality is approached the slope of the Ricci plot gradually decreases, suggesting that there is a maximum value to the Ricci scalar at the origin. This differs from GR, in which the critical solution is singular and the Ricci scalar at the origin increases indefinitely as criticality is approached. We emphasize again that these features are universal.

As shown in Figs. 7 and 8, things are different in 6D. There is no evidence of a radius gap in the radius scaling plots, and the slope of the Ricci plots remains constant until we reach the limits of numerical accuracy. Thus it appears that there is a transition to a new set of scaling exponents, which are plotted in Table II. Note that numerical uncertainties make the first and last entries in each column unreliable. The exponents are different for Ricci and radius scaling, but the absolute values of both appear to increase with decreasing $\tilde{\alpha}$. Moreover a log-log plot of the three reliable radius vs Ricci exponents (Fig. 9) reveals that they are related by

$$\gamma_{(\mathrm{Ricci})} \approx -(2.24 \pm 0.04) \times \gamma_{(\mathrm{Radius})}^{0.28\pm0.02}. \tag{4.5}$$

This is to be compared to the GR case in which the relation is determined purely by the dimension of the two quantities:

$$\gamma_{(\mathrm{Ricci})} = -2\gamma_{(\mathrm{Radius}).} \tag{4.6}$$

Finally, we note that in both 5 and 6D the critical value $A*$ seems to vary linearly with the GB parameter. This is illustrated in Fig. 1.

TABLE I. 5D Ricci scaling exponents in GB region.

$\tilde{\alpha}$	5D Ricci scaling
10^{-6}	-1.426 ± 0.074
5×10^{-7}	-1.573 ± 0.076
10^{-7}	-1.577 ± 0.028
10^{-8}	-3.397 ± 0.049

TABLE II. 6D Ricci and AH radius scaling exponents in GB region.

$\tilde{\alpha}$	6D Ricci scaling	6D radius scaling
10^{-4}	-1.488 ± 0.128	0.257 ± 0.002
10^{-5}	-1.433 ± 0.016	0.207 ± 0.002
10^{-6}	-1.619 ± 0.021	0.313 ± 0.002
5×10^{-7}	-1.814 ± 0.016	0.476 ± 0.002
10^{-7}	-2.029 ± 0.027	0.417 ± 0.002

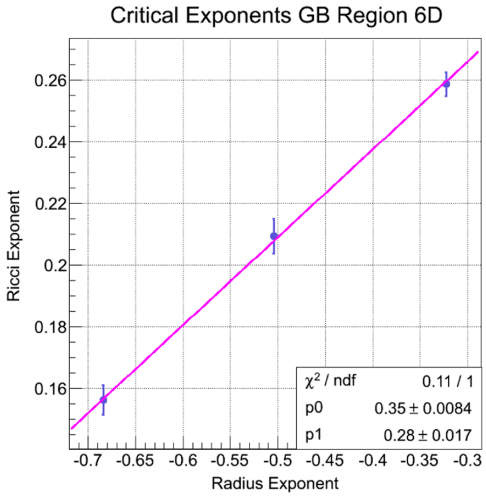

FIG. 9 (color online). Plot of radius exponents vs Ricci (6D).

V. CONCLUSION

We studied the effects of the GB term on the dynamics of the collapse of a massless scalar field minimally coupled to gravity in five and six spacetime dimensions. The GB term destroys the self-similar behavior, as demonstrated by the fact that near criticality the scalar field at the origin oscillates with a constant period. The period in five dimensions is proportional to roughly the cube root of the GB parameter and as the fourth root in six dimensions. While the 5D results differ from those in Ref. [16] it must be emphasized that we have explored a different range of the GB parameter, and this may account for the difference. We are currently investigating modifications to our code in order to extend the range of the GB parameter to overlap that of Ref. [16] so that a direct comparison can be made.

We also showed the existence of modified, but still universal, horizon and Ricci scaling plots near criticality. We found evidence for the existence of a radius gap in five dimensions but not in six dimensions. This qualitative difference is not completely unexpected. As mentioned below Eq. (2.12), the time evolution equation in five dimensions is special, containing one less term than in the higher dimensional cases. It may also be useful to note that qualitative differences exist between five and six dimensions with regard to the stability of black holes under gravitational perturbations [21,22]. Small five dimensional GB black holes are unstable with respect to scalar gravitational perturbations, whereas in six dimensions it is the tensor mode that yields an instability.

It is clearly of interest to confirm our results with further simulations and to try to understand analytically the source of the new scaling behavior.

ACKNOWLEDGMENTS

This work was supported in part by the Natural Sciences and Engineering Council of Canada. It also has been enabled by the use of computing resources provided by WestGrid, the Shared Hierarchical Academic Research Computing Network (SHARCNET: http://www.sharcnet.ca) and Compute/Calcul Canada. T. T. would like to thank the University of Manitoba for funding. We are grateful to Hideki Maeda, Dallas Clement and Patrick Brady for very informative discussions.

[1] C. Lanczos, Ann. Math. **39**, 842 (1938).
[2] D. Lovelock, Aequationes mathematicae **4**, 127 (1970).
[3] D. Lovelock, J. Math. Phys. (N.Y.) **12**, 498 (1971).
[4] D. G. Boulware and S. Deser, Phys. Rev. Lett. **55**, 2656 (1985); B. Zumino, Phys. Rep. **137**, 109 (1986).
[5] R. Zegers, J. Math. Phys. (N.Y.) **46**, 072502 (2005).
[6] S. Deser and J. Franklin, Classical Quantum Gravity **22**, L103 (2005).
[7] D. J. Gross and E. Witten, Nucl. Phys. **B277**, 1 (1986); D. J. Gross and J. H. Sloan, Nucl. Phys. **B291**, 41 (1987); R. R. Metsaev and A. A. Tseytlin, Phys. Lett. B **191**, 354 (1987); B. Zwiebach, Phys. Lett. **156B**, 315 (1985); R. R. Metsaev and A. A. Tseytlin, Nucl. Phys. **B293**, 385 (1987).
[8] M. W. Choptuik, Phys. Rev. Lett. **70**, 9 (1993).
[9] T. Koike, T. Hara, and S. Adachi, Phys. Rev. Lett. **74**, 5170 (1995); arXiv:gr-qc/9607010.
[10] C. Gundlach, Phys. Rev. D **55**, 695 (1997).
[11] J. Ziprick, M.Sc. thesis, University of Manitoba, 2009.
[12] J. Ziprick and G. Kunstatter, Phys. Rev. D **79**, 1 (2009).
[13] M. W. Choptuik, T. Chmaj, and P. Bizon, Phys. Rev. Lett. **77**, 424 (1996).
[14] P. R. Brady, C. M. Chambers, and S. M. C. V. Goncalves, Phys. Rev. D **56**, R6057 (1997).
[15] D. Garfinkle, R. B. Mann, and C. Vuille, Phys. Rev. D **68**, 064015 (2003).
[16] S. Golod and T. Piran, Phys. Rev. D **85**, 104015 (2012).
[17] T. Taves, C. D. Leonard, G. Kunstatter, and R. B. Mann, Classical Quantum Gravity **29**, 015012 (2012).
[18] C. W. Misner and D. H. Sharp, Phys. Rev. **136**, B571 (1964).
[19] H. Maeda, Phys. Rev. D **73**, 104004 (2006); H. Maeda and M. Nozawa, Phys. Rev. D **77**, 064031 (2008).
[20] T. Taves and G. Kunstatter, Phys. Rev. D **84**, 044034 (2011).
[21] R. J. Gleiser and G. Dotti, Phys. Rev. D **72**, 124002 (2005); M. Beroiz, G. Dotti, and R. J. Gleiser, Phys. Rev. D **76**, 024012 (2007).
[22] T. Takahashi and J. Soda, Prog. Theor. Phys. **124**, 711 (2010); **124**, 911 (2010).